

Co., Ltd., Tokyo, Japan, 1979); G. Segrè, H. A. Weldon, and J. Weyers, University of Pennsylvania Report No. UPR-0105T, 1979 (to be published); V. S. Mathur and T. Rizzo, University of Rochester Report No. UR-667, 1979 (to be published); D. Wyler, Phys. Rev. D **19**, 330 (1979).

<sup>3</sup>F. Wilczek and A. Zee, Phys. Rev. Lett. **42**, 421 (1979); A. Davidson, M. Koca, and K. Wali, Phys. Rev. Lett. **43**, 92 (1979), and to be published.

<sup>4</sup>R. Barbieri, R. Gatto, and F. Strocchi, Phys. Lett. **74B**, 344 (1978); R. Gatto, G. Morchio, and F. Strocchi, Phys. Lett. **80B**, 265 (1979); G. Segrè and A. Welson, University of Pennsylvania Report No. UPR-0125T, 1979 (to be published); R. Gatto, in Jerusalem Einstein Centennial Symposium, Jerusalem, Israel, 14-23 March, 1979 (unpublished).

<sup>5</sup>R. N. Mohapatra and D. P. Sidhu, Phys. Rev. D **17**, 1876 (1978); R. N. Mohapatra, in *Proceedings of the Nineteenth International Conference on High Energy Physics, Tokyo, Japan, 1978*, edited by S. Homma, M. Kawaguchi, and H. Miyazawa (International Academic Printing Co., Ltd., Tokyo, Japan, 1979); R. N. Mohapatra and G. Senjanović, Phys. Lett. **73B**, 176 (1978); T. Hagiwara, T. Kitazoe, G. B. Mainland, and K. Tanaka, Phys. Lett. **76B**, 602 (1978).

<sup>6</sup>See, for example, De Rújula, Georgi, and Glashow, Ref. 1, and Mohapatra and Senjanović, Ref. 5.

<sup>7</sup>If  $n_p < n$  it can be trivially shown that either  $\det M = 0$  or the mass spectrum is degenerate.

<sup>8</sup>For example, in the case of three generations we have the mass matrices  $A_3$  and  $A_1 + A_2$  only, as correctly observed by de Crombrugghe in Ref. 1. If nature demands that the  $b$  quark couple significantly to the  $c$  quark, then  $A_3$  is preferred. The general mass matrices containing no disconnected quark families,  $M = A_n$ , have been considered by T. Hagiwara, "Quark Mass Formulae and the Number of Quark Flavors" (to be published). See also H. Fritzsch, CERN Report No. TH-2672, 1979 (to be published).

<sup>9</sup>In general if we diagonalize a Hermitian (complex symmetric) matrix using a bilinear transformation  $U_L A U_R^{-1} = A_D$ , then  $U_R = K U_L$  ( $U_R = K U_L^*$ ), where  $K$  is an arbitrary diagonal unitary matrix that can be absorbed by the quark fields. Then  $\theta_L^i = \theta_R^i$  for both cases and the phases will be related by  $\delta_L^i = \delta_R^i$  ( $\delta_L^i = -\delta_R^i$ ).

<sup>10</sup>In general one cannot absorb all the phases of the unitary matrices for three generations or more. See M. Kobayashi and T. Maskawa, Prog. Theor. Phys. **49**, 652 (1973).

## Multimuon Final States in Muon-Nucleon Scattering at 270 GeV

D. Bauer, J. Kiley, R. Ball, C. Chang,<sup>(a)</sup> K. W. Chen, M. Ghods, S. Hansen,<sup>(b)</sup>  
A. Kotlewski,<sup>(c)</sup> L. Litt,<sup>(c)</sup> and P. F. Schewe<sup>(d)</sup>  
*Michigan State University, East Lansing, Michigan 48824*

and

A. Van Ginneken  
*Fermi National Accelerator Laboratory, Batavia, Illinois 60510*  
(Received 28 June 1979)

Data from a new muon-nucleon scattering experiment includes 513 events, of which 449 are dimuons and 64 are trimuons. Conventional hadronic and electromagnetic processes account for less than 15% of these events. Model calculations suggest that the majority of the dimuons result from associated charm production with a total cross section of about 3 nb.

Events with two (or more) final-state muons have been observed in experiments using muons,<sup>1</sup> neutrinos,<sup>2</sup> or hadrons<sup>3</sup> as incident particles. Possible interpretations of these events in the lepton-scattering experiments include such processes as the production (and semileptonic decay) of charmed mesons,<sup>4</sup> heavy-lepton production and decay,<sup>5</sup> and more conventional hadronic and electromagnetic mechanisms.<sup>1</sup> This Letter describes the characteristics of a large sample of dimuon events from a new muon-scattering experiment. The improved acceptance and increased statistics

of these data have reduced previous uncertainty about the origin of these events.

The experimental apparatus (Fig. 1) consisted of four major parts: the beam, target/calorimeter, final-state muon spectrometer, and trigger/veto counters. The Fermilab muon ( $\mu^+$ ) beam energy was 270 GeV (with a mean spread of 5 GeV) and the intensity within the beam telescope averaged  $6 \times 10^5$  muons/spill with an almost equal number of halo muons outside the beam. This halo was prevented from triggering the apparatus by a large bank of scintillation counters at the

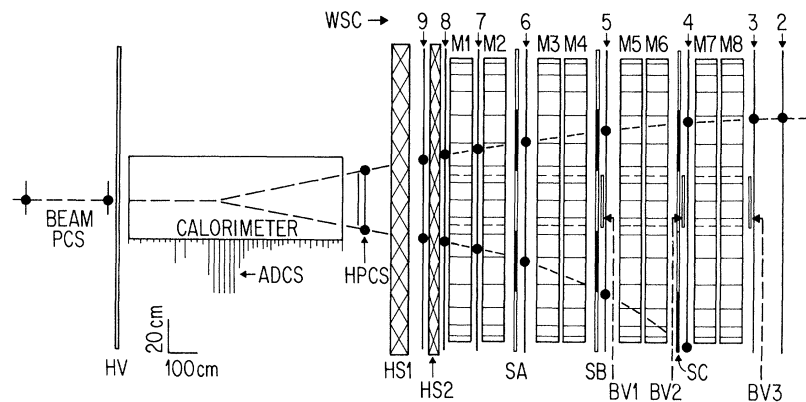


FIG. 1. Layout of apparatus. HV denotes the halo-veto scintillation counters, HPCS are proportional chambers, HS1-2 are steel hadron shields, WSC1-9 are wire spark chambers, M1-8 are iron toroidal magnets, SA, SB, and SC are trigger counter banks, and BV1-3 are beam-veto counters. A dimuon event (OSP) is displayed.

front of the target. The target/calorimeter, a steel-scintillation-counter sandwich with a total length of 738 cm ( $4250 \text{ g/cm}^2$ ), was used to determine the vertex position, the hadron energy, and the number of muons entering and leaving the target. Final-state muons were detected in a large-aperture magnetic spectrometer consisting of toroidal iron magnets, interleaved with wire spark chambers. The field-free region of the toroid holes was filled with heavy concrete to stop penetrating hadrons. The momentum resolution of the spectrometer, about 10% for fully penetrating muons, increased to nearly 40% at the acceptance edges. The front of the spectrometer was equipped with two small proportional chambers to improve multitrack recognition, and two large slabs of steel ( $770 \text{ g/cm}^2$ ) to shield the spark chambers from hadrons. Three banks of scintillation counters were placed within the spectrometer for triggering purposes and three circular veto counters, centered on the magnet holes, rejected events with penetrating particles at small angles.

Multimuon event finding began with reconstruction of all spectrometer tracks for events with a single-beam muon. The distance of closest approach of the incident and scattered muons ( $D_{\min}$ ) defined the event vertex along the beam axis ( $Z_{\min}$ ). Requiring that  $D_{\min} < 10 \text{ cm}$  and  $Z_{\min}$  be within 80 cm of the target effectively eliminated halo contamination. All reconstructed tracks were required to penetrate at least one magnet, imposing a minimum energy of 5 GeV (at the end of the target) on all muons. Events with more than one reconstructed track (about 2% of the total of  $8.2 \times 10^5$  events) were visually scanned to

determine if the tracks constituted a genuine multimuon. Candidates had to have two (or more) good spectrometer tracks coming from a vertex in the target, clear timing information from the trigger counters, and a multiparticle signal from the calorimeter. Reconstruction losses (mainly due to spark-chamber inefficiency) were estimated by scanning 1.5% of the raw data triggers, while multiple scans of most of the multitrack events determined the scanning losses. These checks established an overall finding efficiency of  $(70 \pm 8)\%$  for dimuons and  $(89 \pm 8)\%$  for trimuons.

To label the final-state muons, we define the leading particle ( $\mu_1^+$ ) as the most energetic positive muon, and the produced particle(s) ( $\mu_2^\pm$ ) as the slower positive muon and/or the negative muon. Although multimuon acceptance is complicated by trigger/veto requirements and track curvature in the magnets and is model dependent (due to produced particle correlations), the major features are adequately described by simple energy and angle cuts. Minimum energies, defined by the required range of final-state muons in the spectrometer, are 9 (18) GeV for  $p_1$  and 5 (13) GeV for  $p_2$  corresponding to an interaction at the downstream (upstream) end of the target. Similarly, the angular cuts, defined by the toroid magnet and veto dimensions, are  $13 (8) \text{ mrad} < \theta_1 < 74 (45) \text{ mrad}$ , and  $26 (11) \text{ mrad} < \theta_2 < 144 (64) \text{ mrad}$ .

From the sample with  $1.1 \times 10^{10}$  incident muons, we have found 449 dimuons and 64 trimuons. Application of the finding efficiency corrections increases these numbers to  $644 \pm 55$  dimuons and  $72 \pm 6$  trimuons. Subjecting the leading particles

of multimueon events to the more stringent cuts applied to the deep-inelastic muon sample of  $3.9 \times 10^5$  events gives rates per deep-inelastic scatter of  $(6.3 \pm 0.6) \times 10^{-4}$  dimuons and  $(4.1 \pm 0.4) \times 10^{-5}$  trimuons, uncorrected for the produced muon acceptance.

Full kinematic information is available for 412 dimuon events, of which 298 have particles with opposite charges (OSP), and 114 have particles of the same charge (SSP). Figure 2 compares the characteristics of deep-inelastic scattered muons and leading particles from dimuons. The leading muons prefer lower- $x$  and higher- $y$  regions. The sharp rise in  $W$  seems to be primarily an acceptance effect which masks any possible threshold.

To test various interpretations of multimueons, a Monte Carlo procedure has been developed which, given a model, predicts the rates and kinematic distributions expected in this experiment. The full incident beam distribution is used and all final-state muons are traced through the spectrometer accounting for energy loss, multiple scattering, momentum resolution, and trigger/

veto requirements. Histograms of relevant kinematic variables are produced, weighted by the product of the model cross section and apparatus acceptance. Processes modeled include charm production, dimuons from  $\pi/K$  decay, and elastic Bethe-Heitler trident production. Dimuons arising from the decay of one of the pions (kaons) in the hadron shower, or from prompt muon production, have been calculated in the same manner as in the previous experiment.<sup>6</sup> The number of dimuons predicted from these processes is  $54 \pm 6$ , without finding inefficiency reductions. Dimuon and trimuon rates from elastic Bethe-Heitler muon trident production were calculated using the computer code of Brodsky and Ting for the differential cross section.<sup>7</sup> This process accounts for only  $12 \pm 3$  dimuons and  $8 \pm 1$  trimuons, because the veto severely biases the trigger against low-angle muons. Other potential backgrounds, including vector-meson production, inelastic trident production, and hadronic final-state interactions have been evaluated by Barger *et al.*,<sup>8</sup> whose calculations imply that these processes account for only a small fraction of the ob-

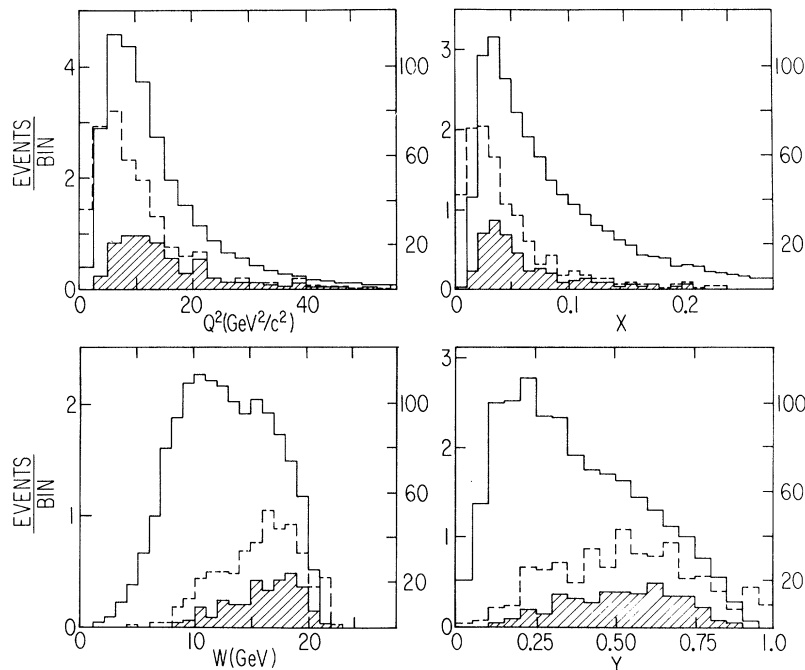


FIG. 2. Histograms of four-momentum transfer squared,  $Q^2 [= 4E_0E_1 \sin^2(\theta_1/2)$ , where  $E_0$  is beam energy and  $E_1$  is scattered muon energy], Bjorken  $x [= q^2/2M\nu$ , where  $\nu = E_0 - E_1$  and  $M$  is nucleon mass], final-state hadron energy  $W [= (2M\nu + M^2 - q^2)^{1/2}]$ , and fractional energy of the virtual photon  $y [= \nu/E_0]$ . The solid histogram represents the deep-inelastic single muons and refers to the arbitrary left scale. The dashed histogram represents the leading muons from the full dimuon sample, while the shaded histogram represents leading muons with the same acceptance as the deep-inelastic sample; both refer to the normalized scale on the right.

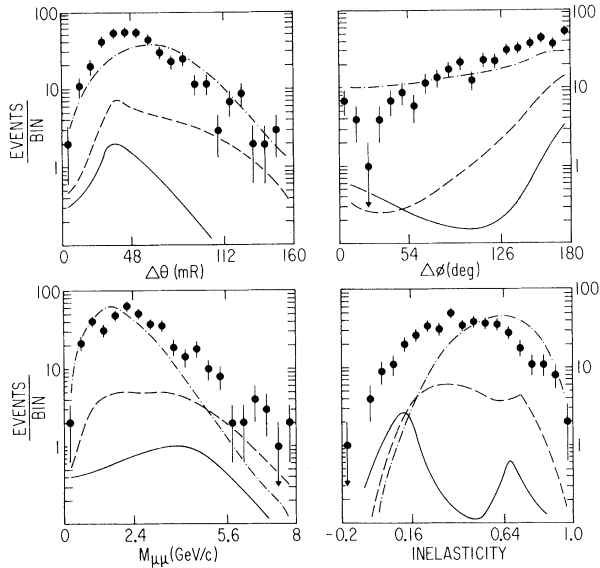


FIG. 3. Combined kinematics of dimuon events, including polar angle difference  $\Delta\theta(=\cos^{-1}[(\vec{p}_1\vec{p}_2)/|\vec{p}_1||\vec{p}_2|])$ , azimuthal angle difference  $\Delta\phi(=\phi_1-\phi_2)$ , apparent mass  $M_{\mu\mu}[=4E_1E_2\sin^2(\Delta\theta/2)]$ , and inelasticity  $[=(E_0-E_1-E_2)/E_0]$ . The dashed curve represents the  $\pi/K$  decay and prompt muon backgrounds and the solid curve represents the elastic Bethe-Heitler trident contribution. The upper (dash-dotted) curve represents the charm-model prediction.

served dimuons.

The charm model (similar to that of Bletzacker, Nieh, and Soni<sup>4</sup> for associated  $D\bar{D}$  production) contains three free parameters governing the normalization and the longitudinal and transverse momentum distributions.<sup>9</sup> With values of these parameters fixed by previous data,<sup>1</sup> the apparatus acceptance in transverse momentum was determined. Unfolding this from the data, with calculated backgrounds subtracted, yields a total cross section for charm production of  $3 \pm 1$  nb, if we assume a branching ratio into muons of 10%. An independent calculation (based on the photon-gluon fusion model) predicts 5 nb, giving some idea of the model dependence.

Figure 3 shows some dimuon kinematic distributions, with curves from the model calculations described above. The pronounced peaking at  $180^\circ$  in  $\Delta\phi$  occurs in all of the calculated processes and represents the tendency of the produced muons to lie along the virtual-photon direction, "back to back" with the scattered muon. The inelasticity favors the production of particles at the hadronic vertex and is inconsistent with background shapes. Further support for the hypoth-

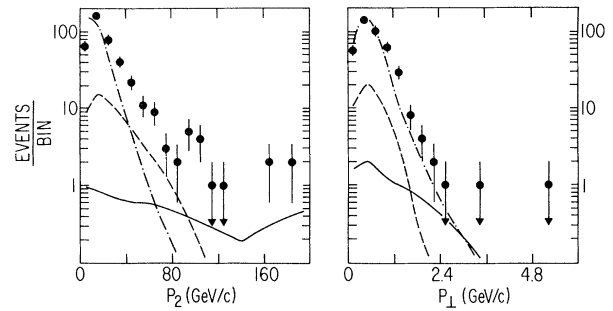


FIG. 4. Produced-particle momentum ( $p_2$ ) and its transverse momentum ( $p_\perp$ ) relative to the virtual photon for dimuons. The curves are as described in Fig. 3.

esis of production and weak decay of heavy hadrons is supplied by the existence of nonzero average missing energy (defined as incident energy minus the sum of final-state energies) which ranges from 9 to 12 GeV as virtual photon energy increases from 25 to 225 GeV. The dimuon produced-particle energy and transverse momentum (relative to the virtual-photon direction) are shown in Fig. 4, and again background shapes do not fit the data distributions. The charm calculation fits reasonably well in transverse momentum (except for a few high- $p_\perp$  events), and not as closely in  $p_2$ . This may indicate some problems with the model used, although the independent calculation<sup>8</sup> follows the same trends.

In summary, the majority of dimuon events in muon scattering appear to result from the associated production and semileptonic decay of charmed mesons. Conventional hadronic and electromagnetic backgrounds are suppressed by the veto and cannot account for more than 15% of the dimuon sample. The small excess of high- $p_\perp$  (and  $-p_2$ ) events may signal the need for more refined model calculations or consideration of new processes.

We acknowledge the support of the Fermilab staff. We also thank M. Brake, M. Kazanski, and B. Spero for their perseverance in the event finding process. This research was supported in part by the National Science Foundation under Grant No. 23365 and by the U. S. Department of Energy under Contract No. E(11-1)-1764.

(a) Present address: National Central University, Chung-Li, Taiwan, Republic of China.

(b) Present address: Fermi National Accelerator Laboratory, Batavia, Ill. 60510.

(c) Present address: University of Miami School of

Medicine, Biscayne Annex, Miami, Fla. 33152.

<sup>(d)</sup>Present address: Brookhaven National Laboratory, Upton, N. Y. 11973.

<sup>1</sup>C. Chang *et al.*, Phys. Rev. Lett. **39**, 519 (1977).

<sup>2</sup>E.g., A. Benvenuti *et al.*, Phys. Rev. Lett. **41**, 725, 1204 (1978).

<sup>3</sup>K. J. Anderson *et al.*, Phys. Rev. Lett. **42**, 944 (1979).

<sup>4</sup>F. Bletzacker, H. T. Nieh, and A. Soni, Phys. Rev. Lett. **37**, 1316 (1976).

<sup>5</sup>Carl H. Albright, Phys. Rev. D **12**, 1319 (1975).

<sup>6</sup>K. W. Chen, in Proceedings of the International Conference on New Particles with New Quantum Numbers, University of Wisconsin, Madison, 1976 (unpublished).

<sup>7</sup>S. Brodsky and S. C. C. Ting, Phys. Rev. **145**, 1018 (1966).

<sup>8</sup>V. Barger *et al.*, Phys. Rev. D **20**, 630 (1979), and Phys. Rev. D, to be published.

<sup>9</sup>K. W. Chen and A. Van Ginneken, Phys. Rev. Lett. **40**, 1417 (1978).

### Measurement of the Branching Fraction for $\tau \rightarrow \rho \nu$

G. S. Abrams, M. S. Alam, C. A. Blocker, A. M. Boyarski, M. Breidenbach, D. L. Burke, W. C. Carithers, W. Chinowsky, M. W. Coles, S. Cooper, B. Couchman,<sup>(a)</sup> W. E. Dieterle, J. B. Dillon, J. Dorenbosch, J. M. Dorfan, M. W. Eaton, G. J. Feldman, H. G. Fischer,<sup>(b)</sup> M. E. B. Franklin, G. Gidal, G. Goldhaber, G. Hanson, K. G. Hayes, T. Himel, D. G. Hitlin,<sup>(c)</sup> R. J. Hollebeek, W. R. Innes, J. Jaros, P. Jenni, A. D. Johnson, J. A. Kadyk, A. J. Lankford, R. R. Larsen, V. Luth, J. F. Martin,<sup>(d)</sup> R. E. Millikan, M. E. Nelson, C. Y. Pang, J. F. Patrick, M. L. Perl, B. Richter, D. L. Scharre, R. H. Schindler, R. F. Schwitters,<sup>(e)</sup> S. R. Shannon,<sup>(a)</sup> J. L. Siegrist, J. Strait, H. Taureg, M. Tonutti,<sup>(f)</sup> G. H. Trilling, E. N. Vella, R. A. Vidal, I. Videau, J. M. Weiss, and H. Zaccone

Stanford Linear Accelerator Center, Stanford University, Stanford, California 94305, and Lawrence Berkeley Laboratory and Department of Physics, University of California, Berkeley, California 94720

(Received 17 August 1979)

This Letter presents a measurement of the decay  $\tau^- \rightarrow \rho^- \nu_\tau$  using data obtained with the Mark II detector at SPEAR. In the center-of-mass energy region  $4.5 \leq E_{c.m.} \leq 6.0$  GeV 85 events are observed in which a charged  $\rho$  was found in coincidence with either an electron or a muon. It was determined that  $B(\tau^- \rightarrow \rho^- \nu_\tau) = (20.5 \pm 4.1)\%$  and the ratio  $B(\tau^- \rightarrow \rho^- \nu_\tau)/B(\tau^- \rightarrow e^- \nu_\tau \bar{\nu}_e) = 1.11 \pm 0.23$ .

The existence of a new charged heavy lepton,  $\tau$ , was first suggested<sup>1</sup> to explain the presence of events in which the only detected particles were an electron and a muon of opposite charge. The experimental evidence accumulated since that time strongly supports this interpretation and there now exists a coherent picture of the  $\tau$  as a sequential heavy lepton with a small- or zero-mass neutrino which couples via the conventional  $V-A$  weak current.<sup>2</sup> In addition there are several precise measurements of the  $\tau$  mass and of branching ratios for leptonic and some hadronic decays.<sup>3</sup> We present below a measurement of the branching ratio for the decay  $\tau^- \rightarrow \rho^- \nu_\tau$  as measured by the Mark II detector at SPEAR.<sup>4</sup> The decay  $\tau^- \rightarrow \rho^- \nu_\tau$  involves only the vector part of the weak hadronic current. Comparison of this measurement with theoretical predictions, based on the coupling of the  $\rho$  to the electromagnetic current, constitutes a test of the validity of the con-

served-vector-current hypothesis (CVC).

The detector has been described elsewhere<sup>5</sup> and we highlight only those detector elements which were crucial to the measurements described herein. The charged tracks were reconstructed from hits in the sixteen drift-chamber layers and photons were detected in the eight liquid argon shower counters which surround the solenoidal coil. Typical photon detection efficiencies exclusive of geometrical effects were 15% at 100 MeV, 50% at 200 MeV, and  $\geq 90\%$  above MeV. Muons were detected in hadron absorption counters consisting of proportional tubes interleaved with iron slabs. The counters have a threshold momentum of 700 MeV/c. Muons headed for these counters which were above this threshold had a  $\geq 98\%$  detection efficiency and the probability that a pion was identified as a muon was 4% at 700 MeV/c, 11% at 900 MeV/c, and 2% above 1.0 GeV/c, at which point the muon has sufficient momentum to